

Article

Numerical Investigation and Optimization of Variable Guide Vanes Adjustment in a Transonic Compressor

Ziyuan Wang ¹, Xiaodong Ren ¹ , Wei Zhu ², Xuesong Li ^{1,*}  and Chunwei Gu ¹¹ Department of Energy and Power Engineering, Tsinghua University, Beijing 100084, China² China North Engine Research Institute, Tianjin 300400, China

* Correspondence: xs-li@mail.tsinghua.edu.cn

Abstract: In the present work, numerical simulation and optimization was carried out to analyze the mechanism of the variable guide vanes (VGVs) of a transonic compressor. A seven-stage transonic compressor including three-stage VGVs was studied. The VGVs were adjusted individually and jointly under different IGV opening degrees. Changes in performance and shock wave were analyzed, and the coupling effect of the VGV joint adjustment was summarized. Aiming at the maximum efficiency, the joint turning angles were optimized. A novel phenomenon was found wherein the VGV adjustment can affect not only its own performance and that of adjacent downstream blades, but also that of upstream blades. Incidence and performance of upstream blades are improved, but those of the VGV and its adjacent downstream blades are deteriorated. VGV adjustment weakens the shock wave and shock-induced boundary layer separation. The optimal solution for VGV joint adjustment is the combination of the optimal solutions for single VGV adjustments. The joint adjustment optimization improves the efficiency by 0.2–1.93% under different IGV opening degrees.

Keywords: variable guide vanes; shock wave structure; stage matching; joint adjustment



Citation: Wang, Z.; Ren, X.; Zhu, W.; Li, X.; Gu, C. Numerical Investigation and Optimization of Variable Guide Vanes Adjustment in a Transonic Compressor. *Energies* **2023**, *16*, 567. <https://doi.org/10.3390/en16010567>

Academic Editor: Alessandro Bianchini

Received: 12 November 2022

Revised: 24 December 2022

Accepted: 30 December 2022

Published: 3 January 2023



Copyright: © 2023 by the authors. Licensee MDPI, Basel, Switzerland. This article is an open access article distributed under the terms and conditions of the Creative Commons Attribution (CC BY) license (<https://creativecommons.org/licenses/by/4.0/>).

1. Introduction

Heavy-duty gas turbines and aero-engines always run under part-load conditions for a long time. As one of the important components of a gas turbine, operation under part-load conditions often leads to a reduction in the performance of the compressor, such as reduced efficiency and reduced stall margin. Therefore, it is necessary to consider the performance of the compressor at part load. At present, variable guide vane (VGV) adjustment in the compressor is one of the widely used methods to change the load. By adjusting the IGV and VGVs, the operating conditions of the compressor can be changed, and the performance of the compressor can be improved by altering its stage-matching relationship.

IGV adjustment mainly changes the gas turbine load by changing the inlet mass flow. Kim [1,2] modeled and studied the part-load performance of a gas turbine and combined cycle, and improved the part-load performance of the gas turbine and combined cycle through IGV adjustment. He [3] analyzed the effect of a variable inlet guide vane (VIGV) on gas turbine performance in an integrated gasification combined cycle (IGCC). For the compressor, the influence of IGV adjustment is reflected in the change of the aerodynamic performance of the IGV itself and the influence on the flow conditions of the downstream rotor. Zimney and Lappi [4] investigated the variation of loss and the flow angle of the IGV, and proposed a loss model and a deviation angle model for the IGV. Banjac et al. [5] developed a performance prediction model for an IGV based on CFD simulation, and predicted its aerodynamic performance. Carcasci [6] calculated the alteration of the flow field when the IGV was adjusted on the Ansaldo Energia AE94.3A compressor. Li [7] focused on adjusting the IGV stagger angle to increase the efficiency of a three-stage, low-speed axial compressor. The maximum efficiency can be improved by about 1% to 3% under different conditions.

With the development of multi-stage axial compressors, the single variable guide vane cannot meet the requirements for efficiency and stall margin of multi-stage axial compressors. The development of variable blades has progressed from a single blade to multi-blades joint adjustment. In the early 1940s, Germany's first turbojet engine, Jumo004, applied the technology of VSV [8]. The stage number of variable stator vanes can reach eight in modern aircraft engines. VGV technology is also used in heavy-dust gas turbines and marine gas turbines, such as the GE 9FA-type gas turbine and PG6541-type gas turbine, the Swiss Sulzer AV series axial compressor, and LM2500 gas turbines [9].

VGV adjustment is used in conjunction with IGV adjustment to change the incidence angle of the compressor and change the stage-matching characteristics, thereby improving efficiency and stall margin. B.A. Jones [10] conducted tests on VGV adjustment for a compressor, and he believed that it was necessary to select the rotation angle of the VGVs based on the matching of the flow angle distribution of the guide vane with the flow angle required by the rotor. Vaclav Cyrus [11] explained the effect of VGV adjustment on compressor separation and stall margin from the incidence angle change. Broichhausen [12] conducted a test on a two-stage transonic compressor to measure the effect on performance and flow field when the VIGV and S1 were adjusted, finding that the S1 adjustment mainly affects the downstream blade, and only affects the upstream blade when the S1 itself is blocked. Kirubakaran [13] performed CFD simulations of a transonic compressor containing three rows of VGVs. It was found that VGV adjustment resulted in an improvement in efficiency and stall margin by avoiding stage-matching problems, and he preliminarily explored the coupling effect of the joint adjustment between VGVs. Li [14] found that the deterioration of the flow in rotor passage in the first two rows was the main problem at partial speeds, and the adjustment of VGVs improved the stage-matching conditions, especially for the first two stages.

A large number of optimizations of VGV joint adjustment based on experiments and modeling calculations have been carried out. Garberoglio [15] conducted experiments on an 11-stage compressor that had four variable guide vanes, and the optimal turning angles were obtained. Ronald [16] carried out throughflow calculation for a five-stage compressor, and found that there are corresponding optimal joint adjustment angles for different rotational speeds. San et al. [17] used an optimization method to obtain the optimal adjustment angle of VGVs at different speeds for a seven-stage axial compressor. The optimization algorithm combining models, including one-dimensional and two-dimensional compressor models and gas turbine models, is also widely used in VGV adjustment angle optimization [18–20].

However, the current study of VGV adjustment is mainly based on the performance obtained from experiments or simplified compressor models, and less consideration is given to the variation of flow field characteristics. Due to the fact that the flow in compressor is always highly nonlinear and three-dimensional, simple overall parameters and zero-dimensional and one-dimensional simplified models have difficulty completely reflecting the flow and performance changes caused by VGV adjustment. 3D internal flow analysis is required. In particular, the first few stages of modern compressors, where VGVs are located, are mostly transonic stages. VGV adjustment will bring shock waves and related structure changes that affect compressor performance, which is less considered in previous work. This will affect our understanding and the application of the effects of VGV adjustment, which is the next work we need to do. On the other hand, the coupling effect in multi-row VGV adjustments is not clear, and the law of the optimal turning angles of VGV joint adjustment is not known from previous work. These require further research to summarize the corresponding laws of VGV joint adjustment to improve the efficiency of the compressor under off-design conditions.

In the present work, a seven-stage axial transonic compressor with three rows of VGVs was investigated, and numerical simulation and optimization aiming at obtaining the maximum efficiency was carried out. The flow mechanism and the law of VGV joint adjustment were studied. First of all, the numerical simulation results were compared with

the experimental results to verify the reliability of the numerical calculations. Secondly, under the fixed IGV opening degree, the performance and the flow variation mechanism of single VGV adjustment at all stages of the compressor were analyzed, focusing on the flow characteristics such as shock wave and boundary layer. Next, considering the coupling effect of VGV joint adjustment, the law of the optimal turning angle was summarized. Finally, the VGV joint adjustment optimization of the compressor was completed. When the gas turbine operates with partial load by changing the IGV opening degree to control the flow, the VGVs can be adjusted according to the scheme in this paper to improve the compressor efficiency.

2. Numerical Methods and Validation

2.1. Multi-Stage Transonic Compressor

A certain seven-stage axial transonic compressor for an industrial heavy-duty gas turbine was studied in this work, whose single passage model is shown in Figure 1. There are 16 blade rows in this compressor, including the inlet guide vane (IGV), three transonic stages, four subsonic stages, and an outlet guide vane (OGV). The rotor tip gap is uniformly 0.5mm for all of the rotors (R1 to R7), which is 0.7% and 1.67% of the chord length of R1 and R7, respectively. Multiple circular arc (MCA) profiles were used for the transonic rotors R1 to R3, while controlled diffusion airfoil (CDA) profiles were used for the rest of the blades. The total pressure ratio of transonic stages is about 1.2–1.3, and the maximum Mach number is about 1.3.



Figure 1. Seven-stage axial transonic compressor.

Three rows of variable guide vanes (VGVs), IGV, S1, and S2, were set in this compressor for operating condition adjustment. For ease of distinction, S1 and S2 will be called VGV1 and VGV2, respectively. The turning direction of the VGVs is shown in Figure 2. With an increase in the turning angle, the opening degree of the VGVs decreases gradually. For example, the IGV turning angle being 0° (abbreviated as $IGV = 0^\circ$) means the IGV is fully open, and $IGV = 40^\circ$ means the IGV is almost closed.



Figure 2. Turning direction of VGVs.

2.2. Numerical Methods

Steady simulation on single passage of the seven-stage compressor was performed in this work. NUMECA FINE/TURBO was used to solve the three-dimensional Reynolds Averaged N-S equations. Real air, rather than ideal gas, was chosen as the work flow to reflect the change in specific heat due to large temperature rises. The Spalart–Allamaras turbulence model was applied to account for the turbulence flow. Central difference method of the finite volume method was used for the space discretization of the equations, and the multi-grid technology was used to accelerate the convergence.

Total temperature, total pressure, and axial flow direction were given at the inlet boundary. Static pressure that satisfies the radial equilibrium equation was set at the outlet boundary, and the operating condition was adjusted by pressure at outlet. No-slip

and adiabatic conditions were imposed on all solid walls (blade, hub, and shroud). One-dimensional non-reflection mixing plane method was applied at rotor/stator interfaces.

The mesh for the simulation was generated using the NUMECA Autogrid5. The grid topology for blade passage adopts the HOH type. The B2B grid was set to periodically match to ensure that the periodic interface was able to accurately transmit shock wave information. The grid at tip clearance adopted butterfly type. For rotor passages, 109 mesh nodes were set spanwise and 17 mesh nodes in tip clearance. The grid number was about 0.9 million in total. For stator passages, 93 mesh nodes were set spanwise and the grid number was about 0.6 million in total. The minimum spacing on the wall was set such that it was sufficiently small enough to satisfy the condition $y^+ < 3$. The overall mesh is shown in Figure 3, and the local mesh is shown in Figure 4.

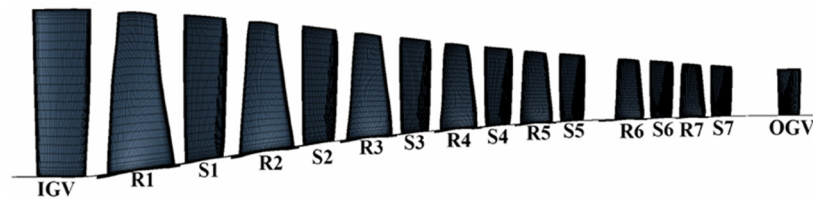


Figure 3. Overall mesh.

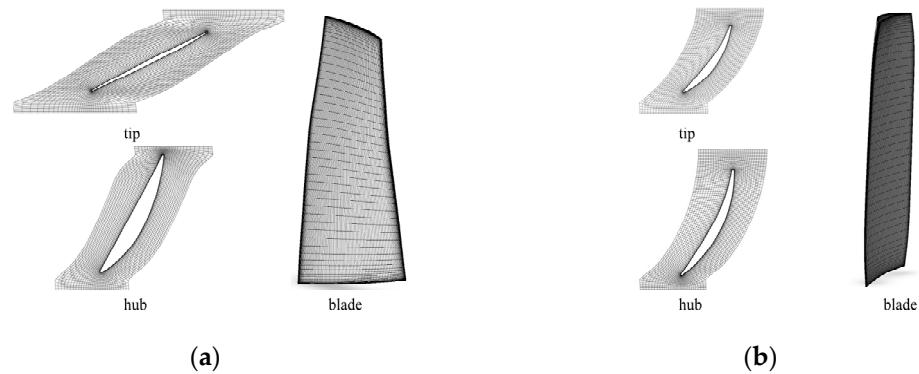


Figure 4. Local mesh of R1 and S1. (a) R1; (b) S1.

Simulation results for four sets of grids were compared, which grids numbered 5.2 million, 8 million, 11 million, and 13.5 million, respectively. The y^+ values of the four sets of grids were all less than 3, which met the requirements of the turbulence model. Figure 5 shows the efficiency curves of these four meshes. It shows that with grid densification, both mass flow and efficiency tend to increase. When the grid number is less than 11 million, the calculation efficiency change is over 0.1%. When the grid number increases to more than 11 million, calculation efficiency changes very little, which is less than 0.05%. In order to ensure the reliability of the calculation results and reduce the calculation cost, 11 million grids were selected for subsequent calculation and analysis.

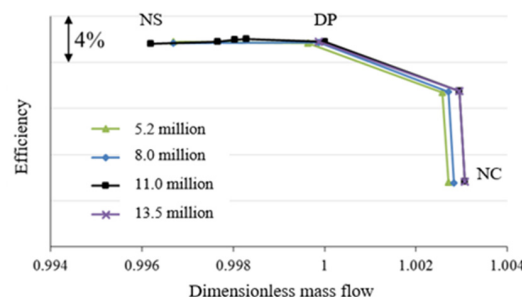


Figure 5. Grid independence.

2.3. Validation

The calculation results were compared with the experimental results. The deviation of mass flow at the design point was about 2.2%, the deviation of pressure ratio was about 0.16%, and the deviation of efficiency was about 0.4%, all within the acceptable range. The pressure distribution between blade rows and the radial distribution of pressure ratio at several cross-sections are shown in Figures 6 and 7, respectively. It is revealed that the calculation results are in good agreement with the experimental results, especially in the mainstream. This shows that the calculation is accurate for the load distribution at all stages and the radial distribution in the blade passages of the compressor. Consequently, the calculation results can accurately simulate the flow in the compressor, which proves the reliability and accuracy of the CFD simulation.

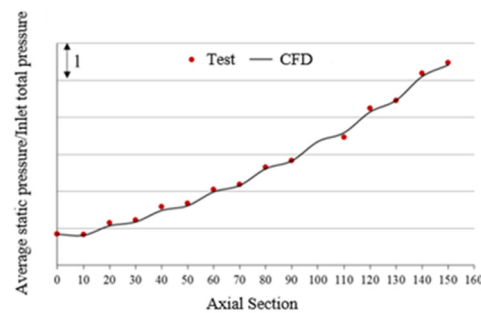


Figure 6. Static pressure distribution between blade rows.

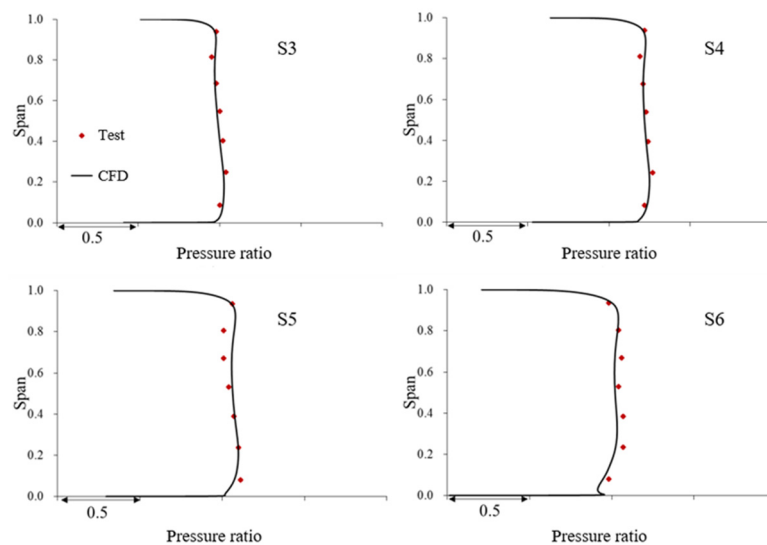


Figure 7. Static pressure spanwise distribution at inlet of stators (static pressure/inlet total pressure).

3. Single VGV Adjustment

In this section, VGV1 and VGV2 were turned respectively under different IGV opening degrees, $IGV = 0^\circ, 10^\circ, 20^\circ, 30^\circ$ and 40° , to investigate the effect of VGV adjustment. For each of certain turning angle combinations, the operating conditions when efficiency is maximum were obtained by changing the static pressure at outlet. Since the condition that $IGV = 0^\circ$ is the design condition, VGVs do not need to be adjusted. Therefore, the condition that $IGV = 0^\circ$ was only used as the reference condition, and VGV adjustment and analysis were not carried out.

3.1. Effect of Performance

3.1.1. Mass Flow

The relationship between IGV turning angle and mass flow is shown in Figure 8. It can be seen that mass flow is not linear with the IGV turning angle. When the IGV turning angle increases by 10° , the mass flow decreases by about 6.4%; when the IGV turning angle increases by 40° , the mass flow decreases by about 35.2%. IGV angle adjustment has a great influence on the mass flow. It is an important method of flow regulation for compressors.

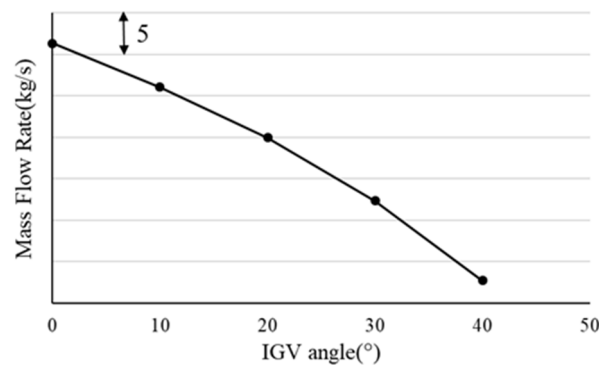


Figure 8. The relationship between IGV turning angle and mass flow.

Under a fixed IGV opening degree, VGV1 and VGV2 are separately adjusted, and the relationship between mass flow and the VGVs' turning angles is shown in Figures 9 and 10. As with the IGV, mass flow is not linear with the VGV turning angle. When the IGV opening degree is constant and only VGV1 is turned, as the VGV1 turning angle changes from 0° to 10° , the mass flow will decrease by about 3.3% when IGV = 10° , while it will decrease by only about 0.4% when IGV = 40° . As IGV opening gradually decreases, VGV1 adjustment will have less impact on the mass flow under the condition of equal angles. In addition, when the IGV is closed to a certain extent, the VGV1 adjustment has little effect on mass flow, and the mass flow is basically unchanged in a large range of turning angles.

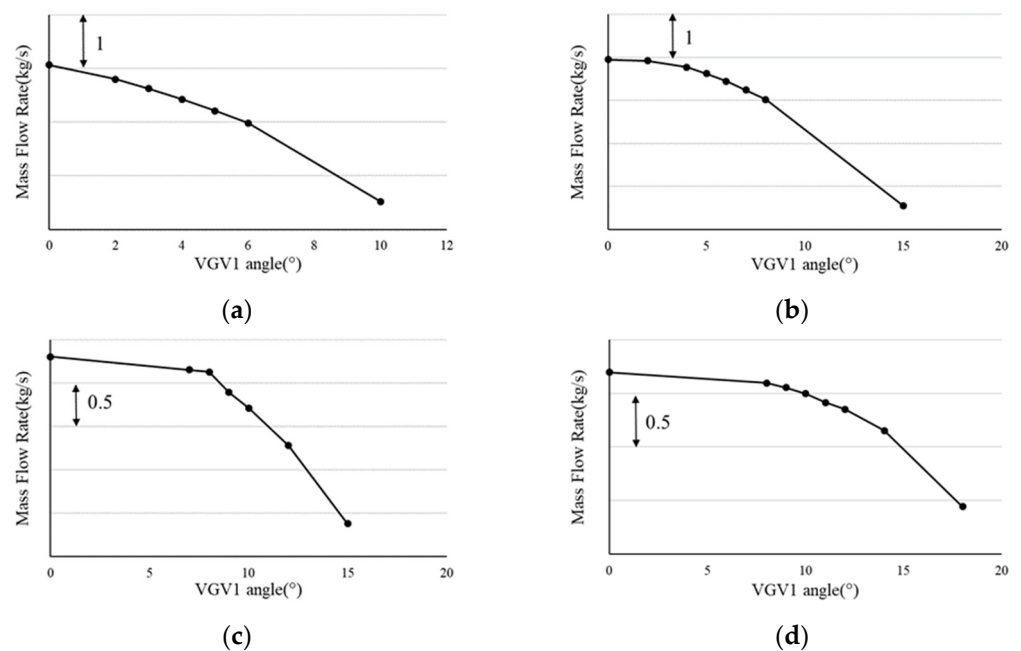


Figure 9. The relationship between mass flow and the VGV1 turning angle. (a) IGV = 10° ; (b) IGV = 20° ; (c) IGV = 30° ; (d) IGV = 40° .

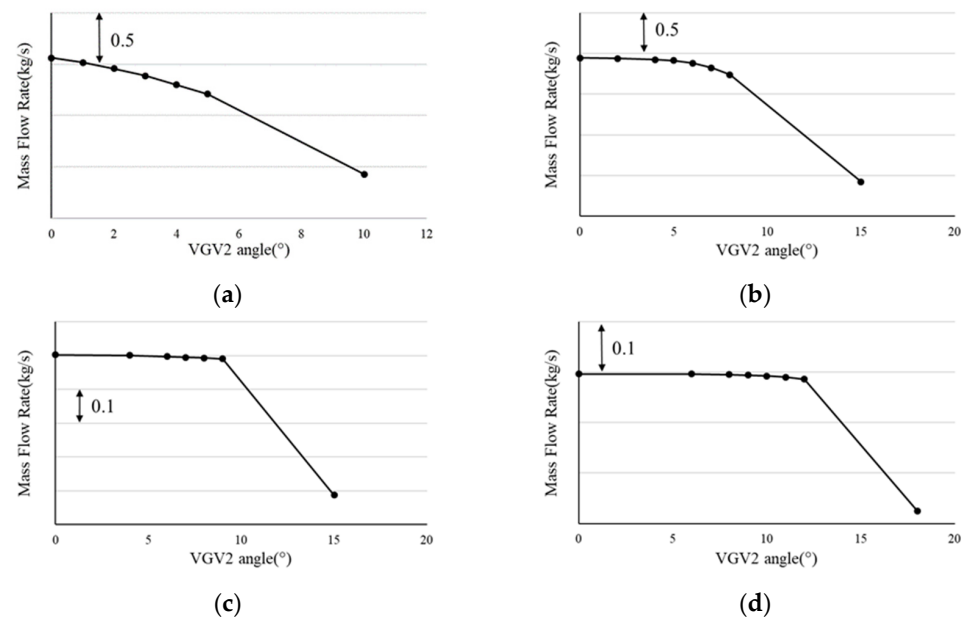


Figure 10. The relationship between mass flow and the VGV2 turning angle. (a) IGV = 10°; (b) IGV = 20°; (c) IGV = 30°; (d) IGV = 40°.

Similar conclusions can be drawn for VGV2. As IGV opening gradually decreases, VGV2 adjustment will have less impact on the mass flow under the condition of equal angles. Meanwhile, compared with VGV1, VGV2 has less impact on mass flow.

Comparing the impact on mass flow between the three rows of variable guide vanes, it is found that IGV has the largest effect on the mass flow, and VGV2 has the smallest effect. This shows that along the flow direction, the VGVs have weaker effect on the mass flow of the compressor. When the IGV is closed to a certain degree, for example, when it is closed to IGV = 40°, the mass flow is basically unchanged in a certain range of the turning angles of VGV1 and VGV2. There is basically no change in the flow rate. The reason is that the mass flow will be restricted only when the VGVs themselves have a blocking effect. When the IGV opening degree is very small, the mass flow is so small that the VGVs can only be closed small enough to form a blocking effect.

3.1.2. Efficiency

The efficiency varying with VGV turning angle under different IGV opening degrees is shown in Figure 11. For a certain IGV opening degree, with the increase in the VGV1 turning angle, the efficiency increases at first and then decreases. There is an optimal VGV1 angle, which is the same for VGV2. The optimal turning angle of VGVs gradually increases as the IGV opening degree decreases. This is because a smaller VGV opening degree matches the smaller mass flow caused by a smaller IGV opening degree.

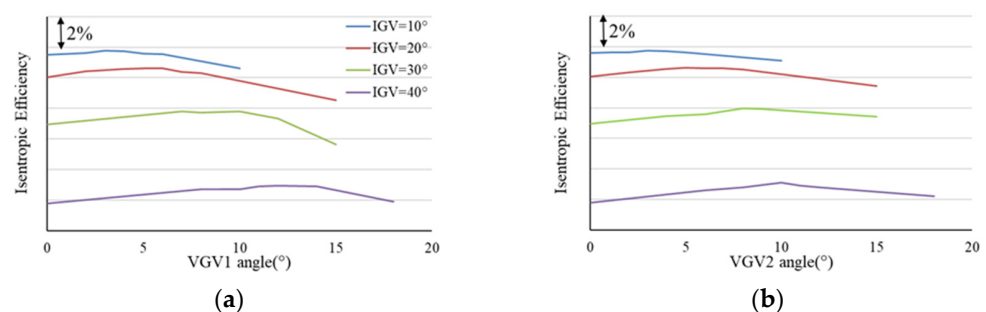


Figure 11. Efficiency varying with VGV turning angle under different IGV opening degrees. (a) VGV1; (b) VGV2.

3.2. Analysis of Mechanism

It is well known that VGV adjustment affects stage-matching characteristics, which affects the performance of stages. Therefore, we first paid attention to changes in incidence angles and the efficiency of all stages. At the same time, the shock wave and boundary layer are also discussed in this section for transonic blades. Because the influence of VGV adjustment on the performance of a compressor is the same under different IGV opening degrees, $IGV = 20^\circ$ is analyzed as the representative in the next section.

3.2.1. Stage/Row Performance

When $IGV = 20^\circ$, performance changes of stages and blades before and after VGV1 adjustment were studied. The original case, $VGV1 = 0^\circ$, and the optimal case, $VGV1 = 6^\circ$, were compared, which is presented in Figure 12. Since the decrease in the IGV opening degree affects the inlet mass flow and the incidence of R1, the efficiency of R1 is low when VGV1 is not adjusted. When VGV1 was turned to 6° , performance changes mainly appeared in Stage 1 and Stage 2, while the rest of the stages were hardly affected. More specifically, in terms of efficiency, for Stage 1, the efficiency of R1 was greatly improved after VGV1 was turned, which was about 7%, while the loss of S1 increased slightly, about 0.005. The combined result was an increase in the efficiency of Stage 1. For Stage 2, there was a moderate decrease in the efficiency of R2. Finally, the efficiency of Stage 2 was moderately reduced. As for pressure ratio, the pressure ratio of Stage 1 decreased, while Stage 2 increased. It is known that VGV1 is S1 of the compressor, R1 is the upstream rotor of VGV1, and R2 is downstream of VGV1. VGV1 adjustment is beneficial to the performance of the upstream stage, but detrimental to the performance of itself and its adjacent downstream stage.

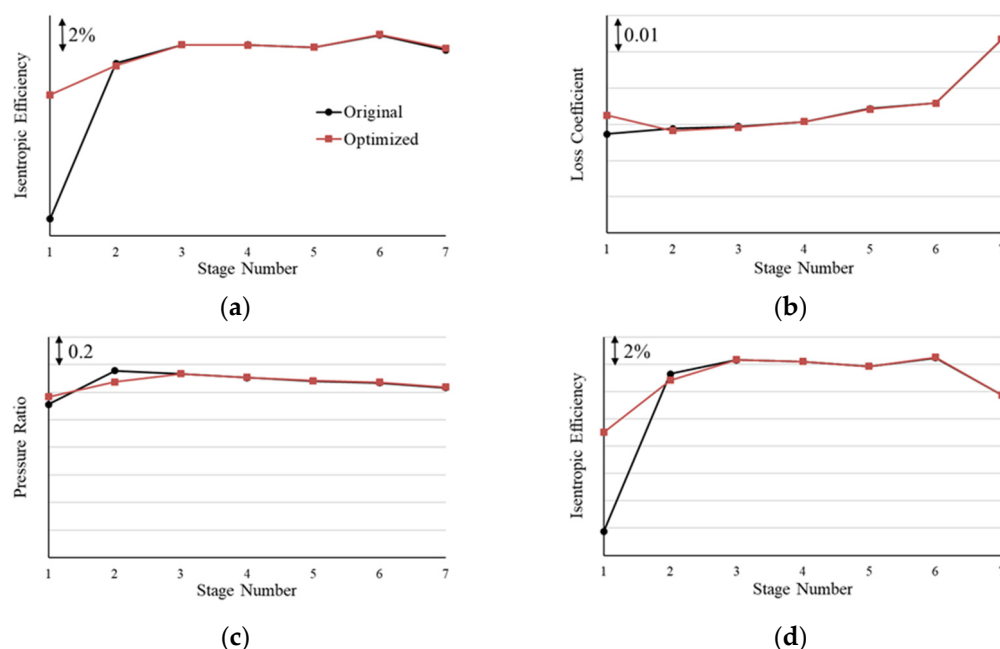


Figure 12. Performance changes of stages and blades during VGV1 adjustment. (a) Efficiency of rotors; (b) loss of stators; (c) pressure ratio of stages; (d) efficiency of stages.

Similar conclusions were drawn when VGV2 adjustment was investigated. Figure 13 shows a comparison between the performance of the original case, $VGV2 = 0^\circ$, and the optimal case, $VGV2 = 5^\circ$, when $IGV = 20^\circ$. The efficiency of R1 and R2 increase, about 3% and 1%, respectively, while that of R3 decreases. Moreover, the loss of S2 increases. When it comes to pressure ratio, Stage 1 and Stage 2 rise while Stage 3 falls. As VGV2 is S2 of the compressor, VGV2 adjustment is beneficial to the upstream stage (which does not have to be adjacent), but detrimental to itself and its adjacent downstream stage.

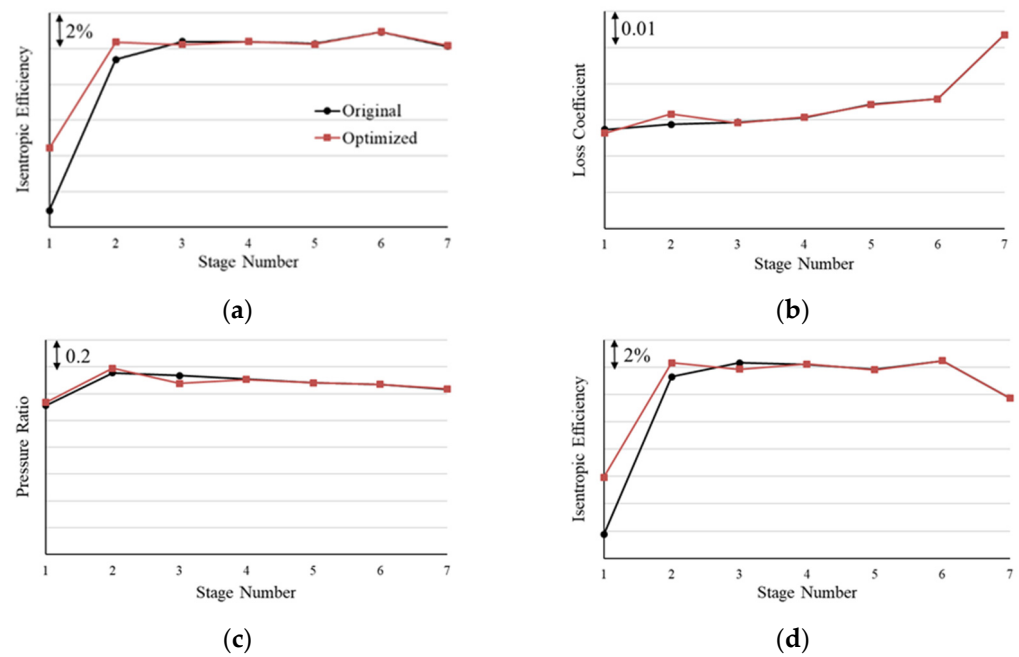


Figure 13. Performance changes of stages and blades during VGV2 adjustment. (a) Efficiency of rotors; (b) loss of stators; (c) pressure ratio of stages; (d) efficiency of stages.

The efficiency spanwise distribution of blades in Stage 1 and Stage 2 when VGV1 is adjusted is presented in Figure 14. The efficiency of R1 increases at all span after VGV1 adjustment. The loss of S1 increases from 0% to 20% span. The efficiency of R2 decreases from 0% to 60% span but increases from 60% to 100% span. The loss of S2 is basically unaffected.

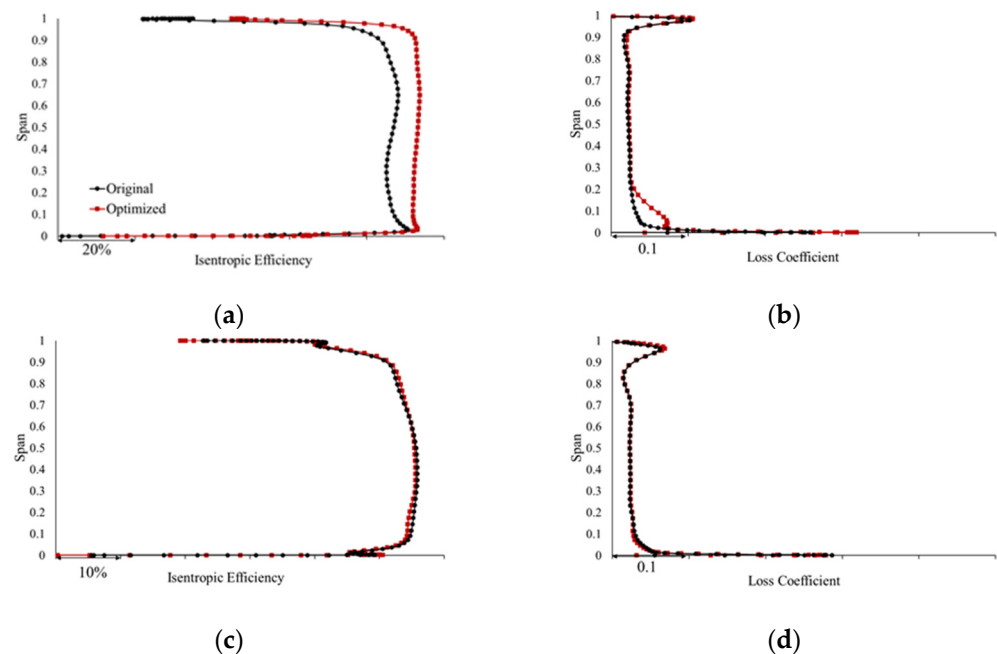


Figure 14. Efficiency spanwise distribution. (a) Efficiency of R1; (b) loss of S1; (c) efficiency of R2; (d) loss of S2.

The pressure spanwise distribution of blades in Stage 1 and Stage 2 when VGV1 is adjusted is presented in Figures 15 and 16. The pressure ratio of R1 increases at all span after VGV1 adjustment. The inlet total pressure of R1 stays constant, while the outlet total pressure rises. The VGV1 adjustment changes the total pressure distribution upstream.

When the VGV1 opening degree is closed, the throat area becomes smaller, and a blocking effect occurs, which causes the upstream total pressure to rise. The inlet total pressure is not affected, and then the pressure ratio of R1 increases. At the same time, a rise in outlet total pressure for R1 leads to a rise in inlet total pressure for R2, while the outlet total pressure of R2 change is small. Consequently, the pressure ratio for R2 decreases after VGV1 adjustment. Total pressure staying constant at the outlet of R2 means that the total pressure ratio of the first two stages remains unchanged. When VGV1 is adjusted, the load of R1 increases and that of R2 decreases. VGV1 adjustment redistributes the load distribution in the first two stages.

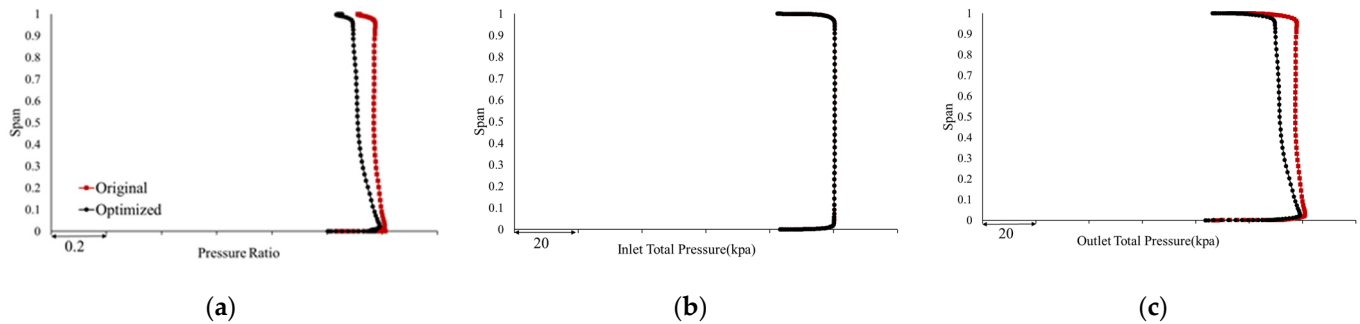


Figure 15. Pressure spanwise distribution of R1. (a) Pressure ratio; (b) inlet total pressure; (c) outlet total pressure.

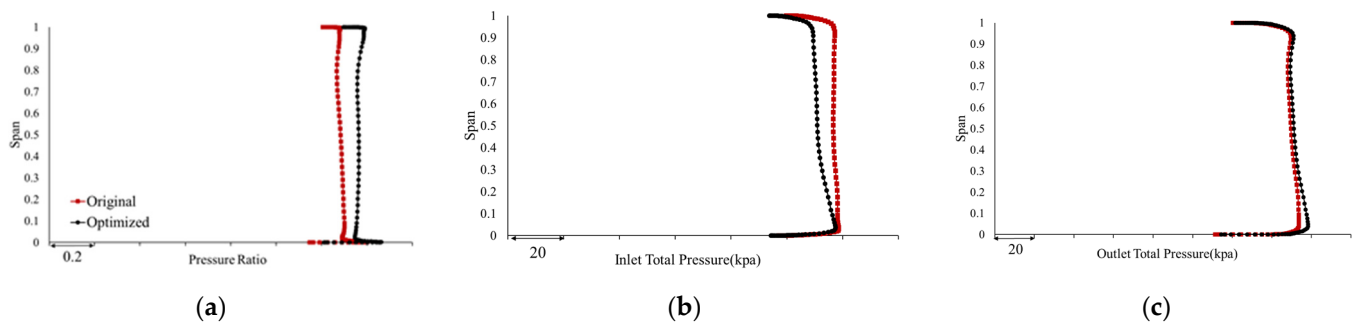


Figure 16. Pressure spanwise distribution of R2. (a) Pressure ratio; (b) inlet total pressure; (c) outlet total pressure.

3.2.2. Incidence

VGV1 adjustment when $IGV = 20^\circ$ was still analyzed as a representative. $VGV1 = -2^\circ, 0^\circ, 2^\circ, 6^\circ,$ and 15° were selected as negative angle, original angle, small angle, optimal angle, and large angle, respectively. At the same time, since blades of the compressor will be in the best state when operating at design point (DP), the distribution of incidence at design point was added, which is regarded as the optimal incidence of the blades. Figure 17 shows the incidence variation. It was found that as the VGV1 turning angle increases, the incidence of R1 moves to positive incidence, S1 and R2 move to negative incidence, and the change of the incidence of each row of cascades shows a translation trend. As VGV1 turning angle increases, the spanwise distribution of incidence of R1 is closer to the incidence of design point. The incidence characteristic is improved, which is beneficial to the improvement of the efficiency of R1. However, the incidence characteristics of S1 and R2 deteriorate, increasing the loss of S1 and reducing the efficiency of R2. In addition, the incidence of S1 and R2 may increase to the stall range of positive and negative incidence, resulting in a mismatch between stages and a sharp drop in efficiency.

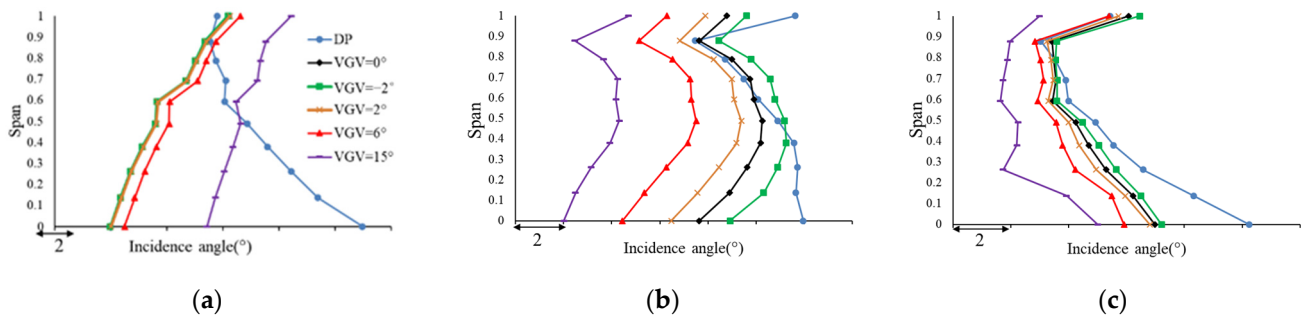


Figure 17. Incidence variation (VGV1 adjustment). (a) R1; (b) S1; (c) R2.

The incidence of VGV1 turned from 0° to -2° and 2° was also compared. During these processes, the turning angle of VGV1 is so small, that the influence on the inlet mass flow is little, for which the relative deviation of the mass flow is calculated to be only 0.023% and -0.04% , respectively. Therefore, the incidence of R1 is basically unchanged. VGV1 adjustment changes the blade inlet angle of S1 and the absolute inlet flow angle of R2, so the incidences of S1 and R2 change, and the direction is opposite. The efficiency changes of the two cases are -0.16% and 0.437% , respectively. There is asymmetry in effect.

When VGV1 is turned from 0° to 15° , the mass flow decreases significantly. The incidence of R1 moves towards a larger positive angle, while incidences of S1 and R2 move towards a larger negative angle. Figure 18 shows the velocity triangle alteration at the inlet of R1 and R2. As for R1, as the VGV1 turning angle increases, the VGV1 opening degree decreases, the inlet mass flow decreases, the inlet axial velocity C_a decreases, and the absolute inlet flow angle α_1 stays constant, so that the relative inlet flow angle β_1 decreases and the positive incidence increases. When it comes to R2, the inlet axial velocity C_a also decreases because of the decrease in the inlet mass flow; however, due to the adjustment of the upstream blade, VGV1, the absolute inlet flow angle α_1 changes, so that the relative inlet flow angle β_1 increases instead, and the incidence increases toward the negative angle. The incidence of R1 is only affected by the change in mass flow, while the incidence of R2 is affected not only by the change in mass flow, but also by the change in the absolute flow angle caused by the adjustment of the upstream VGV. The combined effect of the two causes the incidence to be negative.

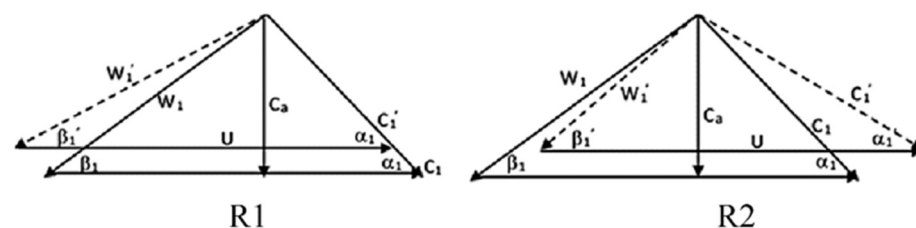


Figure 18. Velocity triangular change at inlet of R1 and R2.

3.2.3. Shock Wave Structure

The first three stages of the compressor investigated in this work are transonic stages, in which the shock wave is one of the important factors affecting the performance. The VGV1 adjustment changes the mass flow and distribution of incidence, which will inevitably lead to alteration in the shock wave structure of rotors, thereby changing the stage performance of compressor. VGV1 = -2° , 0° , 2° , 6° , and 15° under the condition that IGV = 20° were studied.

The isentropic Mach number distribution at 50% span of different VGV1 turning angles is shown in Figure 19. The peak Mach number of the rotors in first three stages are all larger than 1, and a strong shock wave occurs, which causes the interaction between the shock wave and boundary layer, resulting in a large shock wave loss. Due to the IGV opening degree being closed, the shock wave position of R1 moves to trailing edge, and the shock

wave intensity is weaker than that of R2. As the VGV1 turning angle gradually increases from -2° to 15° , the peak Mach number in both R1 and R2 is significantly reduced, and the shock loss will also be reduced.

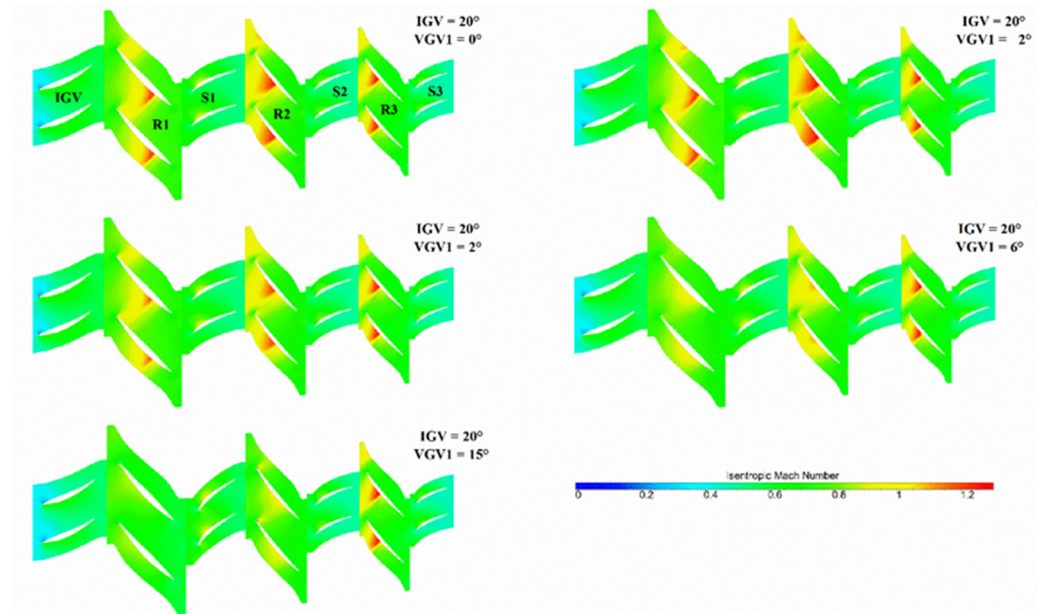


Figure 19. Isentropic Mach number distribution at 50% span (VGV1 adjustment).

The isentropic Mach number distribution on surfaces at 50% span of R1 and R2 is shown in Figure 20. As the VGV1 turning angle increases, the peak Mach number on the suction surface of R1 and R2 gradually decreases, and the position of the peak Mach number gradually moves forward, indicating that not only the intensity of the shock wave is weakened, but also the position of the shock wave moves forward. VGV1 adjustment weakens the intensity of the shock wave, reasonably controls the shock wave position, and effectively suppresses the loss.

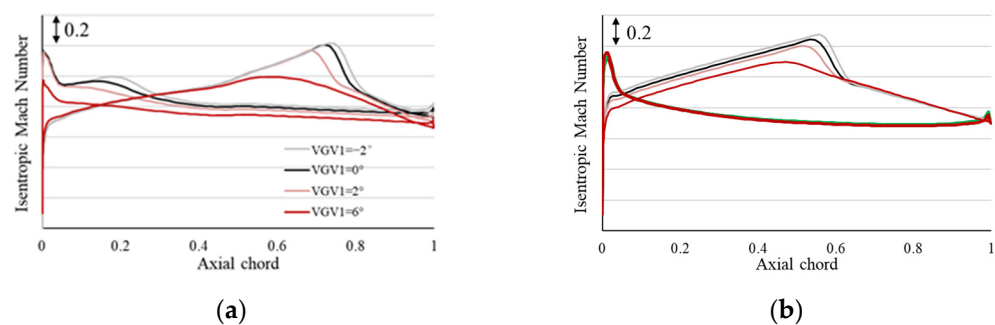


Figure 20. Isentropic Mach number distribution at 50% span (VGV1 adjustment). (a) R1; (b) R2.

Shock intensity and position will affect the interaction between shock and the boundary layer of the blade surface, and this affects the shock-induced boundary layer separation. Limited streamlines on rotor suction surfaces and stator pressure surfaces of the first three stages are shown in Figure 21. When $VGV1 = 0^\circ$, shock-induced boundary layer separation bubbles and radial migration of separation vortices in a large range appear near the trailing edge of R1 root. In addition, there is strong shock-induced boundary layer separation at the tip of R2 near the trailing edge and radial separation at R2 root. Flow fields of other blades are all good. When VGV1 is opened, as $VGV1 = -2^\circ$, the range of separation of R1 and R2 is larger, and the flow field is even worse. When the VGV1 turning angle gradually increases, the shock-induced boundary layer separation of R1 and R2 is continuously

improved, resulting in weaker shock waves. However, when $VGV1 = 6^\circ$, new separation appears on the pressure surface of S1, and it becomes worse as the VGV1 turning angle reaches 15° . Under this condition, the incidence of S1 is so negative that it is unacceptable. The flow fields of other blades have no obvious change.

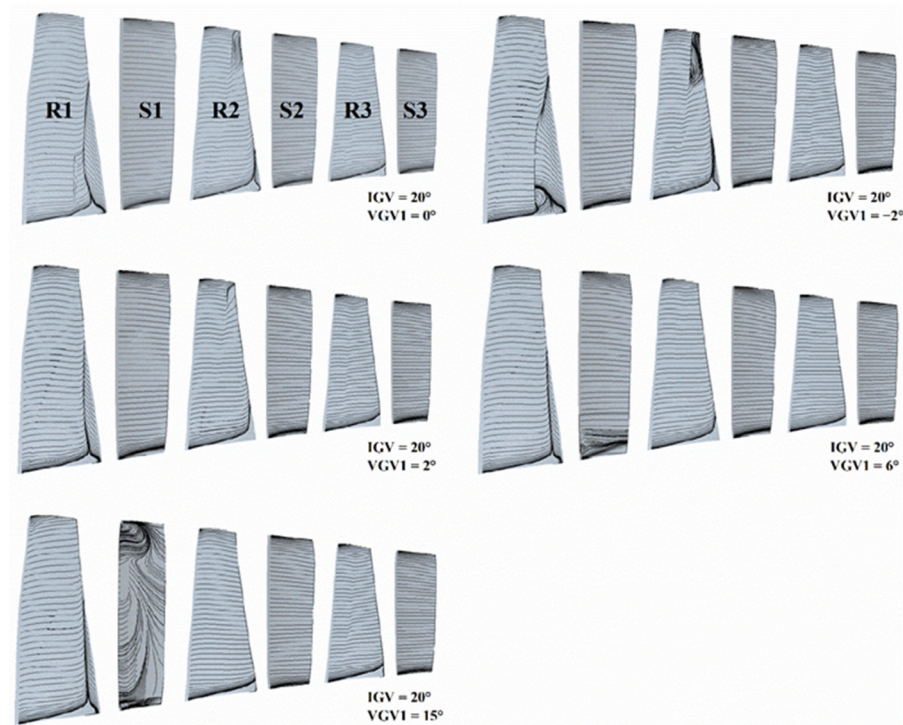


Figure 21. Limited streamlines on blade surfaces of first three stages (VGV1 adjustment).

In conclusion, VGV1 single adjustment changes the inlet mass flow of the compressor, the incidence angles of the upstream and downstream blades, and the peak Mach number on the suction surface of rotors, thus affecting the compressor performance. For R1, which is upstream of VGV1, on the one hand, with the increase in the VGV1 turning angle, the mass flow gradually decreases, resulting in the incidence angle of R1 moving towards the design angle. Therefore, the characteristics of the incidence angle of R1 are improved, which is conducive to improvement in the performance of R1. On the other hand, when the VGV1 turning angle increases, the blockage effect of S1 causes the total pressure at R1 outlet to increase, that is, the pressure ratio increases, which reduces the acceleration process on the suction surface of R1. Thus, the shock wave intensity is reduced, and the shock-induced boundary layer separation phenomenon is significantly improved, which is also conducive to improvement in the performance of R1. Based on the improvement in incidence angle and shock wave structure, the efficiency of R1 is significantly improved. For VGV1 (S1) itself, when the VGV1 turning angle increases, the negative incidence angle of S1 increases, leading to the deterioration of pressure surface separation and increasing loss. For R2, which is downstream of VGV1, on the one hand, the inlet flow angle of R2 is changed after the VGV1 adjustment, which leads to R2 moving towards a larger negative incidence angle and deviating more from the design angle. Therefore, the incidence angle of R2 is deteriorated and the performance of R2 is reduced. On the other hand, the shock intensity of R2 decreases, and the shock boundary layer separation phenomenon is significantly improved, which is conducive to the improvement of R2 performance. At the optimal turning angle, the two effects are relatively balanced and the R2 efficiency is only slightly reduced. VGV2 single adjustment is basically consistent with VGV1.

4. VGV Joint Adjustment

Compared with single VGV adjustment, VGV joint adjustment can coordinate the working conditions of the compressor more effectively, which is the control strategy of the compressor in actual operation. Therefore, it is necessary to study the law and mechanism of variable stator joint adjustment.

4.1. Law of VGV Joint Adjustment

When $IGV = 20^\circ$, the maximum efficiency of the combination of the turning angles in VGV joint adjustment is shown in Figure 22. It is found that the optimal solution for VGV joint adjustment appears in the turning angles of $VGV1 = 6^\circ$ and $VGV2 = 5^\circ$, which is consistent with the optimal solutions of single VGV adjustment above. The optimal solution of VGV joint adjustment is the combination of the optimal solutions of single VGV adjustments.

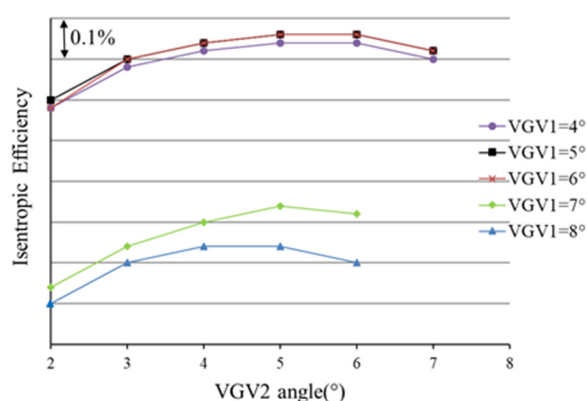


Figure 22. Maximum efficiency of the combination of turning angles in VGV joint adjustment.

The original cases, the optimal turning angles of single VGV adjustments, and the optimal turning angles of VGV joint adjustment, which were named as origin, VGV1-opt, VGV2-opt, and VGVs-opt, respectively, were compared to analyze the impact of VGV joint adjustment on performance. The efficiency of R1, R2, and R3, and the total pressure loss S1 and S2, are shown in Figure 23. Compared with the original, VGV1-opt improves the efficiency of R1, increases the total pressure loss of S1, and reduces the efficiency of R2. VGV2-opt improves R1 and R2 efficiency, reduces R3 efficiency, reduces S1 total pressure loss but increases S2 total pressure loss. VGVs-opt shows higher efficiency than VGV1-opt and VGV2-opt at R1 and R2 efficiency, while S1 and S2 total pressure loss are near the average values of VGV1-opt and VGV2-opt, and R3 efficiency is the same as the VGV2-opt results. The efficiency of VGVs-opt appears as the additive effect of VGV1-opt and VGV2-opt efficiencies.

The incidence spanwise distribution of R1, R2, and R3, and the total pressure loss S1 and S2, are shown in Figure 24. Likewise, the incidence changes of VGVs-opt appear as the additive effect of those of VGV1-opt and VGV2-opt. The incidence movement towards positive angle of R1 for VGVs-opt is larger than those of VGV1-opt and VGV2-opt. R2 coincides with the original, which is near the average value of VGV1-opt and VGV2-opt. R3 is consistent with the result of VGV2-opt. The loss of S1 is near the average of VGV1-opt and VGV2-opt. S2 is consistent with VGV2-opt.

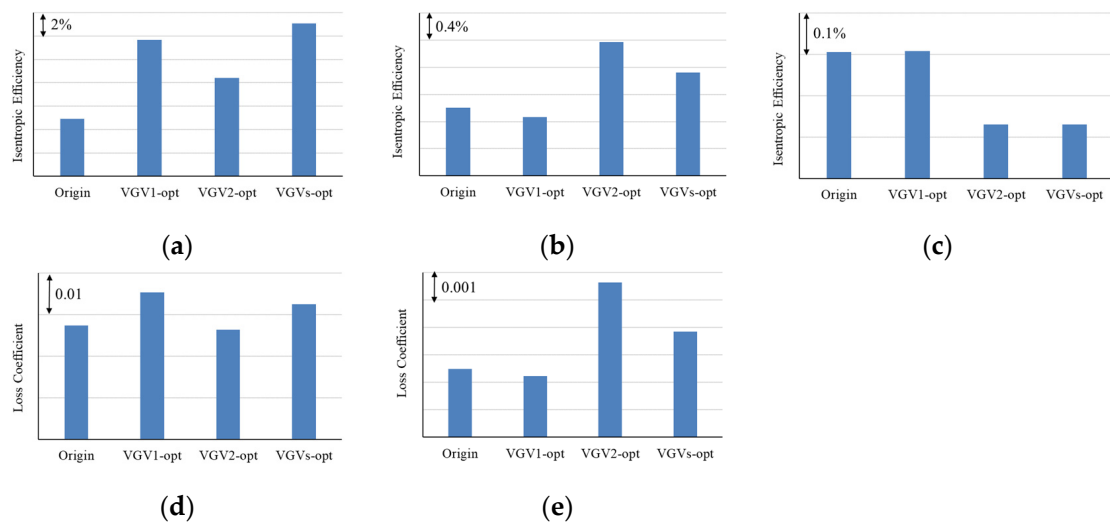


Figure 23. Efficiency of rotors and the total pressure loss of stators (VGV joint adjustment). (a) R1; (b) R2; (c) R3; (d) S1; (e) S2.

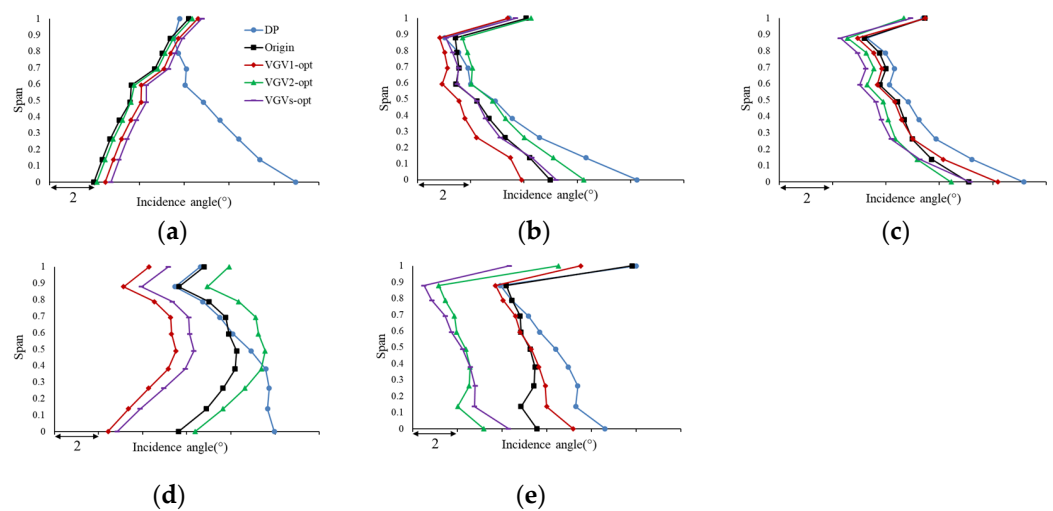


Figure 24. Incidence spanwise distribution (VGV joint adjustment). (a) R1; (b) R2; (c) R3; (d) S1; (e) S2.

The isentropic Mach number distribution of the first three rotors, R1, R2, and R3, is shown in Figure 25. The R1 and R2 peak Mach numbers of VGVs-opt are lower than those of VGV1-opt and VGV2-opt. R3 coincided with VGV2-opt. Correspondingly, the limited streamlines on rotor suction surfaces and stator pressure surfaces of the first three stages are presented in Figure 26. The separation of R1 and R2 of VGV1-opt is improved, but the flow on the pressure surface of S1 is separated. The separation of R1 and R2 of VGV2-opt is also improved, and the flow fields of S1 and S2 do not change significantly. The flow fields on R1 and S1 of VGVs-opt are mainly consistent with VGV1-opt, and the R2 and S2 flow fields are mainly consistent with VGV2-opt. The shock wave structure and the boundary layer separation of VGVs-opt are also the superposition of the VGV1-opt and VGV2-opt.

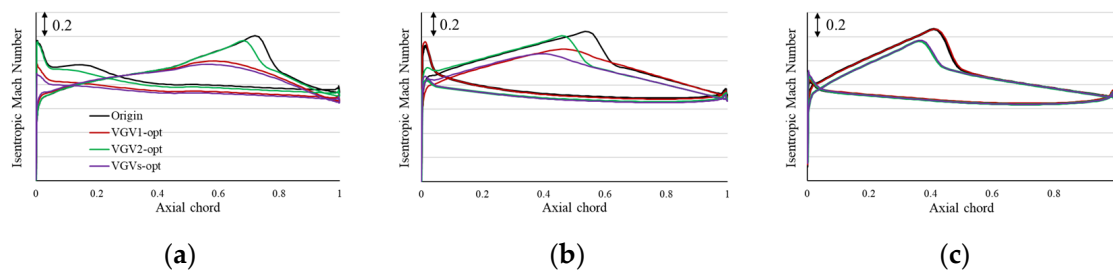


Figure 25. Isentropic Mach number distribution (VGV joint adjustment). (a) R1; (b) R2; (c) R3.

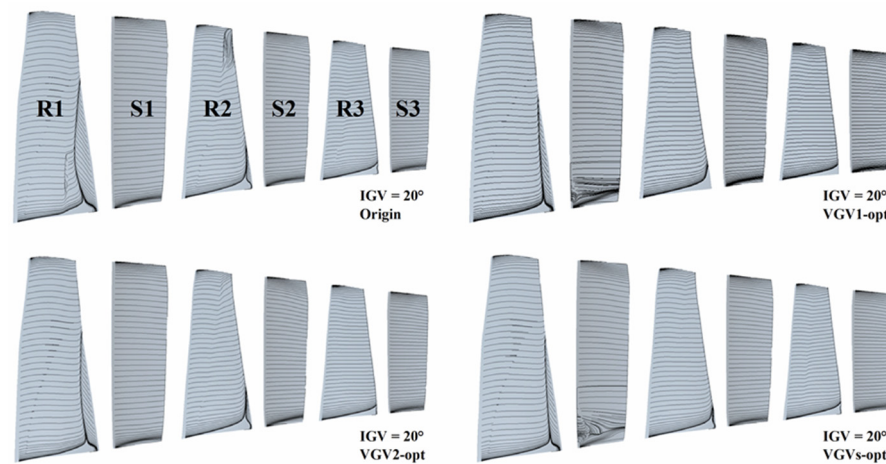


Figure 26. Limited streamlines on blade surfaces of first three stages (VGVs adjustment).

4.2. Performance after Optimization

Based on the conclusions mentioned above and the optimal turning angle of single VGV adjustment, the optimal joint turning angles of VGVs under different IGV opening degrees is shown in Table 1. As the IGV turning angle increases, that is, as the IGV opening degree decreases, the VGVs also change to close, and the turning angle of the downstream VGV does not exceed that of the upstream VGV. The joint turning angles of the VGVs corresponding to other IGV opening degrees can be quickly predicted by referring to the relationship between the IGV opening degree and the optimal turning angle of VGVs in Figure 27.

Table 1. Optimal joint turning angles of VGVs.

IGV (°)	VGV1 (°)	VGV2 (°)
0	0	0
10	3	3
20	6	5
30	10	8
40	12	10

Based on the optimal joint turning angles of VGVs under different IGV opening degrees, simple empirical formulas can be obtained as follows:

$$\text{VGV1} = 0.310 \times \text{IGV}$$

$$\text{VGV2} = 0.257 \times \text{IGV}$$

Obviously, compressor geometry and aerodynamic parameters, such as throat area and wave-front Mach number, will affect the empirical formula. More accurate results can be obtained by taking these into account. However, due to the highly nonlinear flow in the

compressor, the summary of a more general empirical formula requires a lot of additional work, which will not be discussed in this paper. This can be a direction for future research.

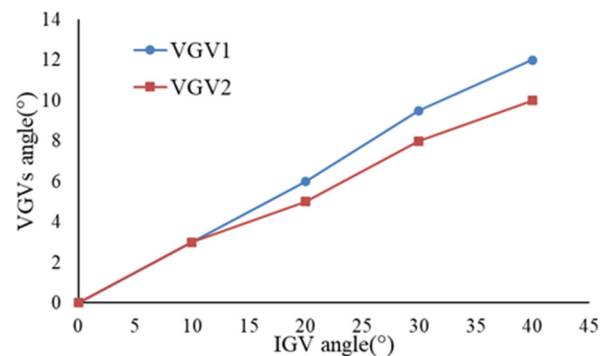


Figure 27. Relationship between the IGV opening degree and the optimal turning angle of VGVs.

Performance curves of the original compressor and the compressor after VGV joint adjustment optimization are shown in Figure 28. When $IGV = 0^\circ$, VGVs are not turned due to good compressor stage-matching characteristics at the design geometry; thus, performance is not improved. The maximum efficiency of other IGV opening degrees are significantly improved, among which the maximum efficiency of $IGV = 10^\circ$ is increased by about 0.2%, $IGV = 20^\circ$ is about 0.66%, $IGV = 30^\circ$ is about 1.5%, and $IGV = 40^\circ$ is about 1.93%, as shown in Figure 29. More efficiency improvement occurs at smaller IGV opening degrees.

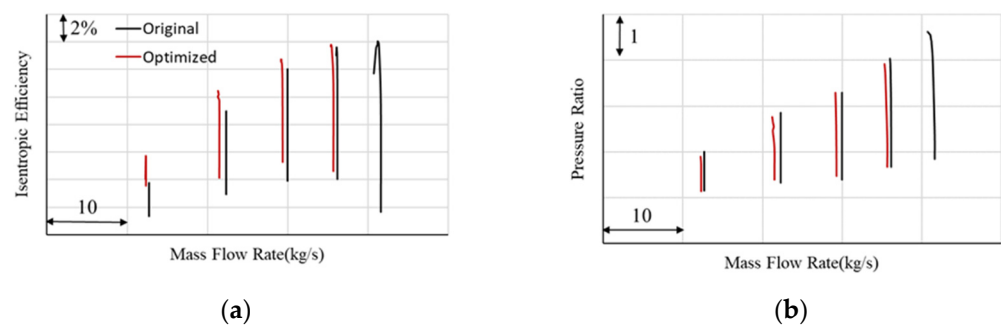


Figure 28. Performance curves of original compressor and compressor after VGV joint adjustment optimization. (a) Efficiency; (b) pressure ratio.

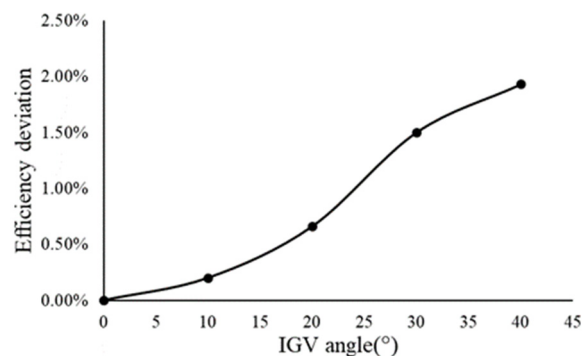


Figure 29. Efficiency improvement varies with IGV opening degree.

5. Conclusions

We conducted numerical simulations on a transonic compressor with different VGV adjustment degrees. The performance variations were studied and the law of VGV joint adjustment was proposed. The following conclusions were drawn.

(1) For some transonic compressors, VGV adjustment affects the performance not only of itself and that of the adjacent downstream blade, but also that of the upstream blade. The load distribution between its upstream and downstream stages is redistributed. Single VGV adjustment is beneficial to the performance of the upstream stage, but detrimental to the performance of itself and that of its adjacent downstream stage. There is a trade-off between improving upstream stage performance and deteriorating its own performance and that of the downstream stage.

(2) VGV adjustment affects the stage-matching characteristics by influencing the incidence and the shock wave structure. On the one hand, the decrease in the VGV opening degree improves the incidence of the upstream rotor, and deteriorates the incidence of itself (stator) and of the downstream rotor. On the other hand, the strength of the shock wave is weakened, and the position of the shock wave is reasonably controlled, which suppresses the loss.

(3) The optimal solution for VGV joint adjustment is the combination of the optimal solutions for single VGV adjustments. Based on this, the optimal solution for VGV joint adjustment was obtained. As the IGV opening degree is turned down, the efficiency improvement after optimization gradually increases. An empirical formula was presented by which the optimal turning angles of VGVs under different IGV opening degrees can be calculated. Compressor geometry and aerodynamic parameters, such as throat area and wave-front Mach number, can be taken into consideration in the future.

(4) When the gas turbine operates with partial load by changing the IGV opening degree to control the flow, the VGVs can be adjusted according to the scheme in this paper to improve the compressor efficiency. When the IGV opening degree is turned down by 10° , the efficiency improvement is about 0.2%, and when the IGV opening degree is turned down by 40° , the efficiency improvement is about 1.93%.

Author Contributions: Conceptualization, Z.W., W.Z. and X.L.; methodology, Z.W. and W.Z.; software, Z.W. and W.Z.; validation, Z.W. and W.Z.; formal analysis, Z.W., W.Z., X.R., X.L. and C.G.; investigation, Z.W., W.Z., X.R., X.L. and C.G.; writing—original draft preparation, Z.W. and W.Z.; writing—review and editing, X.L., X.R. and C.G.; supervision, X.R., X.L. and C.G.; project administration, X.R., X.L. and C.G. All authors have read and agreed to the published version of the manuscript.

Funding: This research was funded by Project 51736008 supported by National Natural Science Foundation of China, and Project 2017-II-0007-0021 of the National Science and Technology Major Project of China.

Data Availability Statement: Not applicable.

Conflicts of Interest: The authors declare no conflict of interest.

Nomenclature

CDA	Controlled Diffusion Aerofoil
CFD	Computational Fluid Dynamics
DP	Design Point
NS	Near Stall
IGV	Inlet Guide Vane
OGV	Outlet Guide Vane
VIGV	Variable Inlet Guide Vane
VGV	Variable Guide Vane

References

- Kim, J.; Kim, T.; Sohn, J.; Ro, S. Comparative analysis of off-design performance characteristics of single and two-shaft industrial gas turbines. *J. Eng. Gas Turbines Power* **2003**, *125*, 954–960. [[CrossRef](#)]
- Kim, T. Comparative analysis on the part load performance of combined cycle plants considering design performance and power control strategy. *Energy* **2004**, *29*, 71–85. [[CrossRef](#)]
- He, F.; Li, Z.; Liu, P.; Ma, L.; Pistikopoulos, E.N. Operation window and part-load performance study of a syngas fired gas turbine. *Appl. Energy* **2012**, *89*, 133–141. [[CrossRef](#)]

4. Zimmey, C.M.; Lappi, V.M. *Data for Design of Entrance Vanes from Two-Dimensional Tests of Airfoils in Cascade*; National Aeronautics and Space Admin Langley Research Center: Hampton, VA, USA, 1945.
5. Banjac, M.; Petrovic, M.V.; Wiedermann, A. A new loss and deviation model for axial compressor inlet guide vanes. *J. Turbomach.* **2014**, *136*, 071011. [[CrossRef](#)]
6. Carcasci, C.; Da Soghe, R.; Silingardi, A.; Astrua, P.; Traverso, S. Heavy Duty Gas Turbine Simulation: A Compressor IGV Airfoil Off-Design Characterization. In *Turbo Expo: Power for Land, Sea, and Air*; American Society of Mechanical Engineers: New York, NY, USA, 2010; pp. 817–824.
7. Li, J.; Lin, F.; Nie, C.; Chen, J. Automatic efficiency optimization of an axial compressor with adjustable inlet guide vanes. *J. Therm. Sci.* **2012**, *21*, 120–126. [[CrossRef](#)]
8. Wiedermann, A.; Frank, D.; Orth, U.; Beukenberg, M. Computational and experimental analysis of an industrial gas turbine compressor. In *Turbo Expo: Power for Land, Sea, and Air*; American Society of Mechanical Engineers: New York, NY, USA, 2011; pp. 319–329.
9. Wang, Z.; Li, J.; Fan, K.; Li, S. The off-design performance simulation of marine gas turbine based on optimum scheduling of variable stator vanes. *Math. Probl. Eng.* **2017**, *2017*, 2671251. [[CrossRef](#)]
10. Jones, B. *Single Stage Experimental Evaluation of Variable Geometry Inlet Guide Vanes and Stator Blading, Part 6 Final Report*; Report No.: NASA CR-54559; National Aeronautics and Space Administration: Washington, DC, USA, 1970.
11. Cyrus, V. Aerodynamic performance of an axial compressor stage with variable rotor blades and variable inlet guide vanes. In *Turbo Expo: Power for Land, Sea, and Air*; American Society of Mechanical Engineers: New York, NY, USA, 1998; p. V001T01A044.
12. Broichhausen, K.-D.; Harster, P. Aerodynamic Analysis of a Two Stage Transonic Compressor with Variable Stator Vanes. In *Turbo Expo: Power for Land, Sea, and Air*; American Society of Mechanical Engineers: New York, NY, USA, 1990; p. V001T01A024.
13. Purushothaman, K.; Naveen Kumar, N.; Pandurangi, V.; Pratap, A. Effect of Stator Variability on Axial Compressor Performance. In *Gas Turbine India Conference*; American Society of Mechanical Engineers: New York, NY, USA, 2019; p. V001T01A005.
14. Li, B.; Gu, C.-w.; Li, X.-t.; Liu, T.-q. Numerical optimization for stator vane settings of multi-stage compressors based on neural networks and genetic algorithms. *Aerosp. Sci. Technol.* **2016**, *52*, 81–94. [[CrossRef](#)]
15. Garberoglio, J.; Song, J.; Boudreaux, W. Optimization of compressor vane and bleed settings. In *Turbo Expo: Power for Land, Sea, and Air*; American Society of Mechanical Engineers: New York, NY, USA, 1982; p. V001T01A034.
16. Steinke, R.J. *Design of 9.271-Pressure-Ratio 5-Stage Core Compressor and Overall Performance for First 3 Stages*; Report No.: NASA TP-2597; National Aeronautics and Space Administration: Washington, DC, USA, 1986.
17. Kim, S.J.; Ki, T. Variable guide vane scheduling method based on the kinematic model and dual schedule curves. *Appl. Sci.* **2020**, *10*, 6643. [[CrossRef](#)]
18. Haglind, F. Variable geometry gas turbines for improving the part-load performance of marine combined cycles–gas turbine performance. *Energy* **2010**, *35*, 562–570. [[CrossRef](#)]
19. Haglind, F. Variable geometry gas turbines for improving the part-load performance of marine combined cycles–Combined cycle performance. *Appl. Therm. Eng.* **2011**, *31*, 467–476. [[CrossRef](#)]
20. Sun, J.; Elder, R. Numerical optimization of a stator vane setting in multistage axial-flow compressors. *Proc. Inst. Mech. Eng. Part A J. Power Energy* **1998**, *212*, 247–259. [[CrossRef](#)]

Disclaimer/Publisher’s Note: The statements, opinions and data contained in all publications are solely those of the individual author(s) and contributor(s) and not of MDPI and/or the editor(s). MDPI and/or the editor(s) disclaim responsibility for any injury to people or property resulting from any ideas, methods, instructions or products referred to in the content.